HHS Public Access

Author manuscript

Photochem Photobiol. Author manuscript; available in PMC 2020 January 01.

Published in final edited form as:

Photochem Photobiol. 2019 January ; 95(1): 364–377. doi:10.1111/php.13002.

Nanolipid Formulations of Benzoporphyrin Derivative: Exploring the Dependence of Nanoconstruct Photophysics and Photochemistry on Their Therapeutic Index in Ovarian Cancer Cells†

Girgis Obaid[1], **Wendong Jin**[1,2], **Shazia Bano**[1], **David Kessel**[3], and **Tayyaba Hasan**[*,1,4]

[1]Wellman Center for Photomedicine, Massachusetts General Hospital and Harvard Medical School, Boston, Massachusetts 02114

[2]Laser Medicine Laboratory, Institute of Biomedical Engineering, Chinese Academy of Medical Science, Peking Union Medical College, Tianjin 300192, China

[3]Department of Pharmacology, Wayne State University School of Medicine, Detroit, Michigan 48201

[4]Division of Health Sciences and Technology Harvard University and Massachusetts Institute of Technology Cambridge, Massachusetts 02139

Abstract

With the rapidly emerging designs and applications of light-activated, photodynamic therapy (PDT)-based nanoconstructs, photonanomedicines (PNMs), an unmet need exists to establish whether conventional methods of photochemical and photophysical characterization of photosensitizers are relevant for evaluating new PNMs in order to intelligently guide their design. As a model system, we build on the clinical formulation of benzoporphyrin derivative (BPD), Visudyne®, by developing a panel of nanolipid formulations entrapping new lipidated chemical variants of BPD with differing chemical, photochemical and photophysical properties. These are 16:0 and 20:0 lysophosphocholine-BPD (16:0/20:0 BPD-PC), DSPE-PEG-BPD and BPD-cholesterol. We show that Visudyne® was the most phototoxic formulation to OVCAR-5 cells, and the least effective was liposomal DSPE-PEG-BPD. However, these differences did not match their optical, photophysical and photochemical properties, as the static BPD quenching was highest in Visudyne, which also exhibited the lowest generation of singlet oxygen production. Furthermore, we establish that OVCAR-5 cell phototoxicity also does not correlate with rates of photosensitizer photobleaching and fluorescence quantum yields in any nanolipid formulations. These findings warrant critical future studies into subcellular targets and molecular mechanisms of phototoxicity of photodynamic nanoconstructs, as more reliable prognostic surrogates for predicting efficacy in order to appropriately and intelligently guide their design.

Graphical abstract

†This article is part of a Special Issue celebrating Photochemistry and Photobiology's 55th Anniversary.

*Corresponding author: thasan@mgh.harvard.edu (Dr. Tayyaba Hasan, PhD).

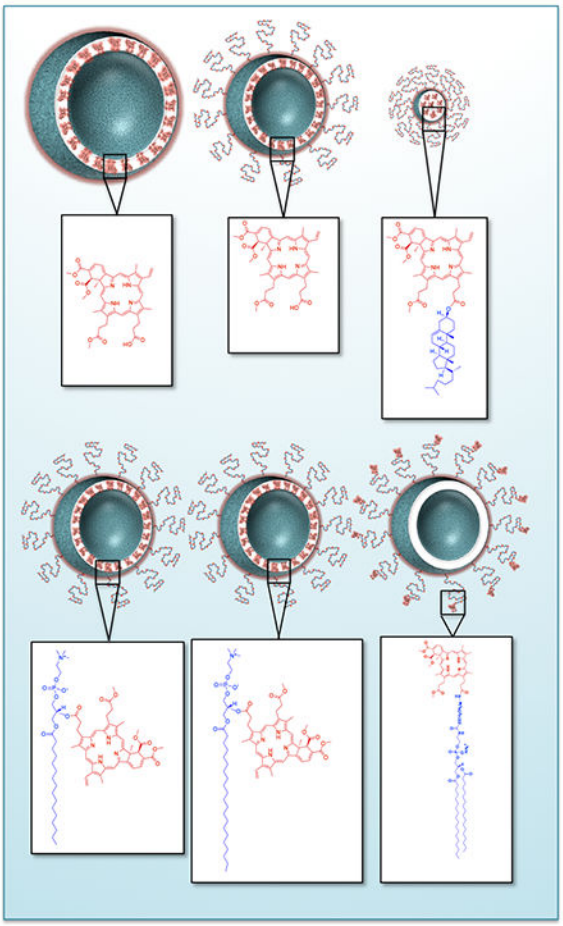

Photophysical and photochemical evaluation of photonanomedicines – light activated nanoconstructs used for photodynamic therapy (PDT) – is considered to be predictive of their potency as photodynamic agents. As a model system, we here prepare a panel of nanolipid formulations of benzoporphyrin derivative and its respective lipidated variants to assess the correlations between the photophysical and photochemical properties, and therapeutic indices in ovarian cancer cells. We concludes that photophysics and photochemistry alone are insufficient to evaluate potency and predict efficacy of emerging photonanomedicines, and that mechanistic insights into subcellular targets must be included in the evaluation process to expedite development and minimize failures.

Keywords

nanolipid; lipid conjugates; photonanomedicine; photosensitizers; photodynamic therapy

INTRODUCTION

Visudyne is the first and only approved photonanomedicine (PNM) formulation, which gained FDA approval for photodynamic therapy (PDT) in 2000 using the photosensitizer (PS) benzoporphyrin derivative (BPD) and formulated with egg phosphatidylglycerol,

dimyristoyl phosphatidylcholine, ascorbyl palmitate and butylated hydroxytoluene (1). Since its approval, Visudyne has set the scene for almost two decades of preclinical and clinical advancements of light activatable nanotechnologies (2–10). Although initially approved for PDT of Wet Age-Related Macular Degeneration (3), the clinical use of Visudyne in oncology is on the rise, with the successful clinical demonstration of pancreatic ductal adenocarcinoma tumor necrosis (2, 11), and recent clinical trials in pancreatic cancer (NCT03033225), prostate cancer (NCT03067051), primary (NCT02872064) and metastatic breast cancer (NCT02939274), and in lung cancer for the PDT-dependent enhancement of liposomal cisplatin delivery (NCT02702700).

BPD, amongst other potent hydrophobic photosensitizers (PSs), such as zinc (II) phthalocyanine and meta-tetra (hydroxyphenyl) chlorin (mTHPC), benefits greatly from nanolipid formulation in constructs, such as liposomes, in order to enhance their water solubility, improve the pharmacokinetic profile and *in vivo* PDT efficacy (12–16). A major motivation for encapsulating hydrophobic PSs in liposomes is to retain their fluorescence activity (photoactivity) and improve the delivery of a photoactive PS, as they typically tend to stack and form J-aggregates in aqueous environments, thus quenching their fluorescence and limiting their photochemical potential.

The chemical modification of photosensitizer molecules has been traditionally leveraged to tune the hydrophobicity and amphiphilicity of the agents to improve their pharmacokinetic profiles and their treatment efficacy for photodynamic therapy (PDT). The lipidation of porphyrins has been previously shown to enable the insertion of these molecules into self-assembled nanolipid formulations including micelles, polymer lipid hybrids and liposomes. Lipid-conjugated porphyrin nanoconstructs have been reported since 2002 (17), with a plethora of elegant recent work on porphysomes, porphyrin lipid-doped liposomes and porphyrin lipid-doped organic nanoconstructs (10, 18, 9).

In this study we have adopted the approach of photosensitizer lipidation to stably formulate BPD into nanoconstructs with varying photophysical and photochemical properties by tethering it to several lipid molecules. These include two lysophospholipids with varying acyl length chains (16:0 and 20:0 lysophosphocholine; PC), to DSPE-PEG_{2000}-NH_2 with a double acyl chain anchor and to cholesterol. Although cholesterol is an unsaturated lipid, with a well-established susceptibility to singlet oxygen-mediated oxidation, it is a potent lipid anchor that has been reported as a stabilizer of therapeutic and diagnostic molecules within nanolipid formulations (19). As a model system controlling for the innate spectral and chemical properties of the photosensitizer BPD, we prepare liposomal formulations (lipo) of native BPD, 16:0 BPD-PC, 20:0 BPD-PC and DSPE-PEG-BPD, in addition to a micellular formulation (mic) of the non-polar, hydrophobic BPD-cholesterol and the clinical nanolipid formulation of BPD, Visudyne (Figure 1). Here we present a full photophysical and photochemical characterization of the nanolipid formulations of BPD and its lipid variants, using methods that are typically reported for evaluating the efficacy of novel nanoconstructs for PDT, (20–26) to explore whether a direct relationship exists between these properties and with phototoxicity in OVCAR-5 ovarian adenocarcinoma cells. We explore one of the fundamental motivations for nanoformulations of hydrophobic photosensitizers, which is the capacity to retain its fluorescence photoactivity in aqueous

environments (8). The rate of PS photobleaching, which has been used in pre-clinical and clinical studies as a prognostic marker for PDT response, is also investigated for all of the nanolipid formulations presented in this study (27, 28). We also asses a critical parameter of the nanolipid formulations, which is the production of singlet oxygen using two probes commonly used to evaluate nanoconstruct photochemistry: the hydrophilic probe singlet oxygen sensor green (SOSG) (20, 21) and the hydrophobic probe diethyl-3-3′-(9,10-anthracenediyl)*bis* acrylate (DADB), which is a lipid membrane-permeable derivative of the more common anthracene-9,10-dipropionic acid (ADPA) (22, 23, 29, 30). Finally, the PDT efficacy of the nanolipid formulations of BPD and its lipidated variants (Visudyne, lipo BPD, lipo 16:0 BPD-PC, lipo 20:0-BPD, lipo DSPE-PEG-BPD, mic BPD-cholesterol; Figure 1) were evaluated in OVCAR-5 cells irradiated with 690 nm light.

Our findings allude to that fact that these photochemical and photophysical properties of nanoconstructs containing photosensitizers are not sufficient to predict their capacity to induce phototoxicity in cancer cells. It is therefore proposed that the efficacy of phototoxicity of PDT nanoformulations is more likely governed by a complex interplay between subcellular localization, molecular targets and mechanistic photochemical cascades. Thus, establishing subcellular targets and mechanisms of cell cytotoxicity is proposed to be a more prognostic approach for evaluating the emerging nanoconstruct designs for PDT-based treatment regimens and must be integrated into the workflow of nanoconstruct design and tuning processes to yield intelligently-prepared photonanomedicines with higher therapeutic indices. This study warrants further investigation into the uptake kinetics, subcellular localization and cell death pathways induced by the panel of nanolipid formulations of BPD and its lipidated variants presented here as a model system to further understand the relationship between the physical properties of photosensitizer conjugates and the molecular biology of PDT in cancer.

MATERIALS AND METHODS

Synthesis of the BPD lipid conjugates.

- ***Benzoporphyrin derivative conjugates of 16:0 lyso PC, 20:0 lyso PC and cholesterol***: The carboxylate of the benzoporphyrin derivative photosensitizer was coupled to the hydroxyl moiety of the phospholipid 1-palmitoyl-2-hydroxy-sn-glycero-3-phosphocholine (16:0 lyso PC) through an ester bond, using Fischer esterification, according to an adaptation of our previously reported protocol (5). Briefly, 16:0 lyso PC (99.13 μl, 25 mg/ml stock in chloroform, 495.63 g/mol; Avanti® Polar Lipids, Inc.) was placed in a 13 × 100 mm Pyrex® tube and the chloroform was evaporated using a flow of nitrogen gas through a 16 gauge needle. The photosensitizer benzoporphyrin derivative monoacid ring A (BPD, verteporfin, mixed isomers, 17.97 mg, 718.79 g/mol; U.S. Pharmacopeia (USP®)) was added to the dried 16:0 lyso PC. 1-ethyl-3-(3dimethylaminopropyl) carbodiimide (EDC, 38.81 mg, 155.24 g/mol ; Sigma-Aldrich), 4-(dimethylamino)pyridine (DMAP, 15.27 mg, 122.17 g/mol; Sigma-Aldrich), and N,N-Diisopropylethylamine (DIPEA, 52.25 μl, 129.24 g/mol. 0.742 g/ml; Sigma-Aldrich) were then added to the dried 16:0 lyso PC and BPD

mixture. The ratio of 16:0 lyso PC : BPD : EDC : DMAP : DIPEA was 1 : 5 : 50 : 25 : 300. The mixture was dissolved in dichloromethane (DCM, 5 ml, ACS Reagent Grade, 99.5%; Sigma-Aldrich) and rigorously stirred at 2500 RPM for 24 h at room temperature in the dark using a magnetic stir plate. The 16:0 lyso PC-BPD lipid conjugate (16:0 BPD-PC) was purified using Analtech Preparative Thin Layer Chromatography Silica Uniplates (Sigma-Aldrich) running on a mobile phase consisting of 10% methanol in DCM. The 16:0 BPD-PC-containing silica fraction (Rf = 0.144) was removed from the TLC plate, placed in a 50 ml polypropylene tube (Corning®), and extracted from the silica fraction by sonication in 33% methanol in DCM (30 ml) for 10 min. The silica was sedimented by centrifugation at 3,000 xg for 10 min and the supernatant containing the extracted 16:0 BPD-PC was collected into a 250 ml round-bottom flask. The silica fraction was washed as such with 33% methanol in DCM two further times and all 16:0 BPD-PC solutions were pooled into the 250 ml round bottom flask. The solvent mixtures were removed from the extract by rotary evaporation under reduced pressure at 40°C connected to a liquid nitrogen trap condenser. Residual silica that previously dissolved in the methanol-DCM solvent mixture was removed by redissolving the dried 16:0 BPD-PC extract in 100% DCM. The insoluble silica precipitate was removed by filtration using a Fisherbrand™ poly(tetrafluoroethylene) (PTFE) filter (0.22 μm pore size, 13 mm diameter; Thermo Fisher Scientific) driven by a gastight glass syringe. The DCM was removed from the filtered 16:0 BPD-PC solution using rotary evaporation as described earlier. The purified conjugate was then redissolved in chloroform (5 ml) and stored in the dark at −20°C. The concentration of the 16:0 BPD-PC was determined by diluting the phospholipid conjugate in DMSO and measuring the UV-Visible absorption spectrum using an extinction coefficient $\varepsilon_{687\ nm}$ = 34,895 $M^{-1}.cm^{-1}$. The lysophospholipid 1-arachidoyl-2-hydroxy-sn-glycero-3-phosphocholine (20:0 lyso PC) and cholesterol were both conjugated to BPD using the same procedure and the same reaction stoichiometry. All lipidated BPD variants were validated with MALDI using 3,4-dihydroxybenzoic acid (10mg/ml in ethanol; Sigma Aldrich) as a matrix. 16:0 BPD-PC expected M.W. is 1196.41 g/mol, observed is 1197.123 m/z; 20:0 BPD-PC expected M.W. is 1252.52 g/mol, observed is 1255.715 m/z; BPD-cholesterol expected M.W. is 1087.43 g/mol, observed is 1085.287 m/z.

- ***Benzoporphyrin derivative conjugate of DSPE-PEG_{2000}-NH_2***: BPD was conjugated to DSPE-PEG_{2000}-NH_2 using EDC amide coupling. Briefly, DSPE-PEG_{2000}-NH_2 in chloroform (0.896 μmol) was mixed with a 10-fold molar excess of BPD in chloroform (8.96 μmol) and a 5-fold molar excess of EDC to BPD (44.8 μmol) in a 13 × 100 mm Pyrex® tube. The mixture was stirred in the dark at 2500 RPM for 24 hours. The chloroform was then evaporated using a flow of nitrogen and the dry reaction mixture was dissolved in 1ml methanol. The reaction mixture was then run through Sephadex® LH-20 (GE Healthcare Life Sciences) equilibrated with methanol, and the fastest running colored fraction consisting of DSPE-PEG_{2000}-BPD was collected. The methanol was

evaporated, and the DSPE-PEG_{2000}-BPD was dissolved in chloroform (5 ml) and stored in the dark at −20°C. The DSPE-PEG_{2000}-BPD conjugate was validated with MALDI using 3,4-dihydroxybenzoic acid (10 mg/ml in ethanol; Sigma Aldrich) as a matrix. The expected M.W. is 3479.25 g/mol, observed is 355.481 m/z. This discrepancy is due to the normal size distribution of all PEG chains conjugated to DSPE, which only exists as a polydisperse polymer with an average molecular weight of *ca.* 2,000 g/mol, and thus the expected M.W. of DSPE-PEG-BPD is only an approximation.

HPLC purity analysis of BPD and its lipidated variants was performed using Abs_{435nm} of the Soret Band. Analytical HPLC cycles were ran using a gradient increasing from 95% water : 5% acetonitrile to 5% water : 95% acetonitrile over 30 min, followed by a 30-minute hold at 5% water : 95% acetonitrile. In the case of BPD cholesterol, the organic mobile phase flow was held for a total of 60 min to allow for full elution of the hydrophobic conjugate.

Nanolipid formulations of BPD.—BPD, 16:0 BPD-PC, 20:0 BPD-PC and DSPE-PEG-BPD were formulated into liposomes using the thin lipid film hydration process. DPPC, Cholesterol, DOPG, and DSPE-$mPEG_{2000}$ in chloroform were mixed at a molar fraction ratio of 0.58 : 0.08 : 0.29 : 0.05 in cholesterol and was doped with either 0.3 mol% BPD, 0.3 mol% 16:0 BPD-PC, 0.3 mol% 20:0 BPD-PC and or 0.15 mol% DSPE-PEG-BPD in chloroform. The solvent was evaporated under nitrogen flow and the film was further dried under vacuum. The lipid films were hydrated in PBS at 42°C with 5 freeze-thaw-vortex cycles. The lipid mixtures were then extruded eleven times through two 100 nm polycarbonate membranes to prepare unilaminar liposomes. These preparations are referred to as lipo BPD, lipo 16:0 BPD-PC, lipo 20:0 BPD-PC and lipo DSPE-PEG-BPD.

BPD-cholesterol was formulated into micelles by mixing 23 nmoles of the conjugate in chloroform with 10 mg DSPE-$mPEG_{2000}$. The solvent was evaporated under nitrogen flow and the film was further dried under vacuum. The lipid mixture was hydrated in 1 ml of 1×PBS and the sample was vortexed for 5 min and sonicated for 1 h in the dark. The micellized formulation was filtered twice through 0.22 μm cellulose filters and stored at 4°C in the dark. This preparation is referred to as mic BPD-cholesterol.

Visudyne solutions was prepared by hydrating the lyophilized clinical powder preparation in sterile 1×PBS with gentle agitation. All BPD-containing preparations were quantified with visible absorption spectrophotometry using $\varepsilon_{687\ nm}$ = 34,895 $M^{-1}.cm^{-1}$ and were stored at 4°C in the dark. Hydrodynamic diameter, polydispersity indices and ζ-potential of the nanolipid formulations were determined by a Zetasizer Nano ZS Dynamic Light Scattering Instrument.

Optical characterization.—UV-Visible absorption spectrophotometry using an Evolution 300 UV-Vis Spectrophotometer was used to determine BPD equivalent concentrations using $\varepsilon_{678\ nm}$ 34,895 $M^{-1}.cm^{-1}$. The Soret band was not used for quantitation of BPD equivalent concentrations to avoid any interference with the absorption of lipid constituents in the UV-violet regions of the spectrum. All free PS preparations and nanolipid formulations of BPD

and its lipidated variants were dissolved in DMSO for UV-Visible absorption spectrophotometry to maintain the same solvent used to calculate the extinction coefficient of BPD (31). In DMSO, no changes in the Q-band absorption maxima or width of the Q-band are observed after lipidation, suggesting that the extinction coefficient is consistent after lipidation (see Supporting Information, Figure S2). Dissolution in DMSO is also performed in order to disassemble the nanoformulations and prevent light scattering from interfering with the absorption measurements. For the remaining fluorescence-based optical characterization methods, the free PS preparations of BPD and its lipidated variants were solubilized in DMSO, while nanolipid formulations were all prepared in PBS to evaluate their absolute emission when formulated in intact constructs. Fluorescence emission spectra of all samples containing BPD and BPD variants were collected using SpectraMax M Series Multi-Mode Microplate Reader with an excitation wavelength of 435 nm. The same procedure for measuring fluorescence was used for the photobleaching studies, where all free molecule preparations and nanolipid formulations of BPD and its lipidated variants were irradiated at 150 mW/cm^2 of 690 nm light with total fluences of up to 100 J/cm^2.

Fluorescence polarization of free PS molecules in DMSO or nanolipid formulations in PBS were performed using a Beacon 2000 Fluorescence Polarization apparatus at 37°C using an excitation wavelength of 400 nm and collecting emission from 660-700 nm.

Singlet oxygen measurements.

- ***Singlet Oxygen Sensor Green (SOSG):*** Preparations of 1μM BPD equivalent of BPD and its lipidated variants, either free in DMSO or formulated into nanoconstructs in PBS (100 μl) were mixed with 10 μl of 50 μM SOSG (Thermo Fisher Scientific) in 96 well plates (black wall, transparent base) in repeats of 4 wells. The solutions were irradiated with a 690nm laser at 150 mW/cm^2 with fluences of 0, 2.5, 5, 10, 15, 25, 75 and 100 J/cm^2. Following each individual dose application, the fluorescence intensity was measured using a SpectraMax M Series Multi-Mode Microplate Reader using 460 nm excitation and a 515 nm cut-off filter, collecting emission at 525nm for the nanoformulations in PBS, or using 480 nm excitation and a 515 nm cut-off filter, collecting emission at 555 nm for the free molecules of BPD and its lipidated variants in DMSO.
- ***diethyl-3-3′-(9,10-anthracenediyl)bis Acrylate (DADB):*** DADB was prepared as described before.(30) Solutions of 2 μM equivalent of BPD and its lipidated variants, either free in DMSO or formulated into nanoconstructs in PBS (50 μl) were mixed with 50 μl of 10 μM DADB either in DMSO or in PBS, respectively, in 96 well plates (black wall, transparent base). The wells were irradiated at 690 nm at an irradiance of 150 mW/cm^2 with fluences of 0, 2.5, 5, 10, 15, 25, 75 and 100 J/cm^2 . Every time after irradiation, the fluorescence intensity was measured using an excitation of 405 nm and a 475 nm cut-off filter, collecting emission at 505 nm for the nanoformulations in PBS and at 535 nm for BPD and its lipidated variants as free molecules in DMSO.

Culturing and PDT of OVCAR-5 cells.—OVCAR-5 cells were cultured in T75 canted neck, cell culture flasks (Corning) at 37°C and 5% CO_2. RPMI media, supplemented with

10% heat-inactivated fetal bovine serum (FBS, Gibco) and 1× Penicillin/Streptomycin was used to culture the cells. OVCAR-5 cells at 80–90% confluence were trypsinized, counted and seeded in 96, black-walled, transparent base plates (Corning) at a density of 1,500 cells/well. The following day, nanolipid dilutions as per PDT dose product of 10 −5000 (nM × J/cm^2) for lipo BPD, mic BPD-cholesterol and Visudyne and a dose product of 25 −15000 (nM × J/cm^2) for lipo 16:0 BPD-PC, lipo 20:0 BPD-PC and lipo DSPE-PEG-BPD. To achieve these dose products, nanolipid formulations were prepared in the RPMI media and incubated with cells for 24h at 37 °C. The cells were then washed three times with culture media to remove liposomes not internalized by the cells, replaced with fresh culture media and irradiated using 690 nm laser at an irradiance of 150 mW/cm^2 and the aforementioned PDT dose products (nM × J/cm^2). Table 1 outlines the concentrations of BPD equivalent necessary and the light doses chosen to achieve the PDT dose product mentioned.

Following PDT, the cells were incubated for a further 72 hours prior to assessing the viability using 3-(4,5-Dimethylthiazol-2-yl)-2,5-Diphenyltetrazolium Bromide (MTT, Sigma-Aldrich). The media was replaced with fresh cell culture media containing MTT (0.1 mg/ml), incubated for 1 hour at 37 °C and was then removed from the cells. The formazan was dissolved in DMSO (100ul) and the absorbance was measured at 517 nm. Viability was calculated as a percentage absorbance at 517 nm with respect to untreated controls.

RESULTS AND DISCUSSION

Lipidation of BPD and stable insertion into nanoformulations

BPD was lipidated by Fischer esterification of the PSs carboxylate and the alcohol groups of 16:0 lyso PC, 20:0 lyso PC and cholesterol. BPD was also conjugated to DSPE-mPEG$_{2000}$ by amide coupling. The purified lipidated variants were characterized by MALDI to verify their molecular weight and by HPLC to assess purity (Figure S1, Table 2). Exact molecular weights in g/mol that are expected when analyzing the molecular weights using MALDI were calculated using ChemDraw Professional v15.1. PEGylated liposomal formulations of BPD, 16:0 BPD-PC, 20:0 BPD-PC and DSPE-PEG-BPD were prepared using the thin film hydration method and are respectively referred to as “lipo” preparations. All BPD and its lipid variants were inserted into liposomal formulations at 0.3 mol% of the total lipid content, other than DSPE-PEG-BPD, which was inserted at 0.15 mol%. As a result of the terminal tethering of hydrophobic BPD on the polar PEG-modified head groups of the liposomes, visible aggregation of the nanolipid formulation was observed when the DSPE-PEG-BPD was inserted into liposomes at a mol% exceeding 0.15 mol%.

Due to the absence of polarity of BPD-cholesterol, which exists in both parent molecules BPD (carboxylate) and cholesterol (alcohol), stable membrane entrapment into liposomal bilayers was not feasible and the conjugate precipitated upon hydration of the lipid films with 1×PBS. To circumvent the need for polarity for stabilization into a nanolipid formulation, the BPD-cholesterol conjugate was micellized using DSPE-mPEG$_{2000}$ in PBS to form the resultant micellular nanolipid formulation, termed mic BPD-cholesterol. Visudyne solutions in PBS were prepared from the lyophilized clinical preparation and used without further processing. After lipidation, the BPD variants exhibited no shift in the Q-band absorption maxima when fully dissolved in DMSO and exhibited no broadening of the

Q-band with a full-with half maximum of 20 nm, suggesting that the extinction of the BPD molecule is unaltered by lipidation (Figure S2).

Physical characterization of nanolipid formulations

The hydrodynamic diameter, polydispersity indices and ζ-potential of the nanolipid formulations of BPD and its lipidated variants were characterized by dynamic light scattering, as summarized in Figure 2 and Table 3. Figure 2a) shows that lipo BPD, lipo 16:0 BPD-PC and lipo 20:0 BPD-PC are almost identical in size with a hydrodynamic diameter of *ca.* 110 nm. Lipo DSPE-PEG-BPD is *ca.* 50 nm larger with a hydrodynamic diameter of 159.63 nm and mic BPD-cholesterol is the smallest with a mean hydrodynamic diameter of 42.42 nm. The hydrodynamic diameter of Visudyne varied hugely, ranging from *ca.* 200 nm – 1 μm, with a mean of 733.78 nm and standard deviation of 488.87 nm. All nanolipid formulations were relatively monodispersed with a polydispersity index (P.D.I.) below 0.2, aside from Visudyne and mic BPD-cholesterol which had mean P.D.I. values of 0.66 and 0.48, respectively. The P.D.I. is a measure of the size distribution that is proportional to the width of the dispersity of sizes in a nanoconstruct preparation with a Gaussian size distribution, divided by the average size in that sample. The greater the P.D.I., the greater the dispersity of sizes within that sample (32). Both Visudyne and mic BPD-cholesterol formulations had neutral ζ-potentials, whilst the lipo BPD, lipo 16:0 BPD-PC, lipo 20:0 BPD-PC and lipo DSPE-PEG-BPD were all anionic with ζ-potentials ranging from −17 mV to −20 mV, that are known to exhibit favorable circulation half-lives and the lower clearance by the liver, compared to cationic and neutral nanolipid formulations (33, 34).

Optical characterization

Being one of the key motivations of formulating hydrophobic PSs, such as BPD, into nanoconstructs, such as the nanolipid preparations in this study, is to maintain their solubility in aqueous environments in order to retain their photoactivity. The fluorescence emission spectra (650 nm to 750 nm) of BPD and its lipid variants, free in DSMO or encapsulated into nanolipid formulations in PBS, were measured using an excitation wavelength of 435 nm. Fluorescence photoactivity is presented in Figure 3 as a percentage of the respective unquenched molecule in DMSO, derived using the equation below:

$$Photoactivity = \left(\frac{fluorescence\ emission\ intensity\ at\ maximum\ of\ \ formulation\ in\ PBS}{fluorescence\ emission\ intensity\ at\ maxima\ of\ \ free\ variant\ in\ DMSO} \right) \times 100$$

Given, that the fluorescence quantum yield of the lipidated BPD variants is almost identical to the native BPD when dissolved in DMSO, it is unlikely that changes in photoactivity following integration into the nanolipid formulation are due to increased triplet yields but are rather more likely due to static quenching. Interestingly, BPD was in the highest quenched state (91.17% quenched) when formulated in Visudyne (Figure 3a). lipo 16:0 BPD-PC was the most effective at retaining photoactivity of the PS with only 14.4% quenching. The degrees of retention of the photoactivity of BPD and its lipidated variants by the nanolipid formulations are summarized in Table 4, where the fluorescence quantum yields are also calculated using BPD in methanol as a reference (35).

Fluorescence Polarization: Fluorescence polarization (P) is defined by the following equation, where F_L is the fluorescence emission intensity that is parallel to the plane of excitation light, and F_D is the fluorescence emission intensity that is perpendicular to the plane of excitation light (36).

$$P = \frac{(F_L - F_D)}{(F_L + F_D)}$$

Fluorescence polarization is used extensively as a sensitive measure of the immediate environment of a fluorophore at the nanoscale and also reports on the degree of rotational freedom the molecule has. In this study, we used fluorescence polarization as an indirect measure of the reduction in rotational freedom of BPD following lipid conjugation and as a validation of the extent of integration into the nanoformulations. We found that for all the lipidated BPD variants, the polarization values in DMSO are increased with respect to native BPD, showing that 16:0 BPD-PC has the highest polarization at 7.3 mP. As anticipated, polarization further significantly increased with incorporation into the nanoformulations for all preparations, with lipo DSPE-PEG-BPD being the highest at 250 mP (Figure 4). It was not possible to determine an accurate fluorescence polarization value for Visudyne due to the highly quenched state of the BPD molecule when the formulation is suspended in PBS.

Fluorescence Photobleaching as an Indirect Indicator of Reactive Molecular Species Production

Photobleaching of a fluorophore often refers to a pathway for excited state deactivation;(37) however, in the context of PDT, permanent photobleaching refers to the process by which reactive molecular species generated by an excited PS, such as singlet oxygen and free radicals, react with the PS itself causing it to degrade into smaller molecule fragments that no longer exhibit the same absorption profile or photochemical activity (38–40). In the clinic, the photobleaching of photosensitizer fluorescence within irradiated tissue is used as an indicator of responsiveness to PDT and is therefore one of the metrics leveraged to guide dosimetry (28, 41, 42). Other PDT dose metrics include tissue uptake of PSs, light tissue penetration measurements, tissue oxygenation, transient changes in light penetration through tissue, self-shielding of PSs and photochemical depletion of oxygen at high fluence rates (42). *In vitro,* photobleaching of BPD *in situ* within 3D nodules of OVCAR-5 cells was used to report a measure of “effective” PDT dose that positively correlated with PDT efficacy (27). In another report, the percentage of photobleaching of BPD *in situ* within 3D nodules of OVCAR-5 cells also correlated with tumoricidal potency of the PDT regimen (43). However, the concept of using photobleaching as a measure of PS potency is paradoxical, in that a PS that is rapidly photobleached is also no longer capable of generating cytotoxic reactive molecular species (RMS). Thus, if the PS is present in a microenvironment that promotes self-degradation by photobleaching, the availability of the RMS to induce therapeutic cytotoxic effects could also be hindered. This can be the case for PSs such as BPD and its lipidated variants in the nanolipid formulations where vicinal lipid constituents of the encapsulating nanoformulation can become oxidized by the RMS generated upon

photoirradiation, subsequently inducing photobleaching of the same PS shortly after (Figure 5a).

In this study, we explore the rates of photobleaching of BPD and its lipidated variants, both free solubilized in DMSO, or entrapped in the nanoformulations. BPD is known to predominantly produce singlet oxygen as a type II reaction product; however, type I reactions have also been reported, with the generation of hydroxyl radical, which may be quenched by the DMSO used to solubilize the hydrophobic free molecules of BPD variants (44, 45). As this study is aimed at exploring the impact of photobleaching rates of the nanoformulation of BPD and its lipidated variants on cellular phototoxicity, potential quenching of hydroxyl radicals by DMSO will have no further repercussions within the context of this study. It is important to note that the conjugation of BPD to 16:0 PC, 20:0 PC, DSPE-mPEG$_{2000}$ and cholesterol causes no variations in rates of photobleaching, which remain at *ca.* 1 nM/s (Figure 5b). When formulated into the nanolipid formulations, the rate of photosensitizer photobleaching increases in Visudyne, lipo 16:0 BPD-PC, lipo 20:0 BPD-PC and mic BPD-cholesterol, with respect to the free molecules. The rate of photobleaching of BPD and DSPE-PEG-BPD was largely unaffected by formulation in liposomes. Interestingly, the fastest rate of photobleaching was observed with Visudyne (4.97 nM/s), where we hypothesize that the highly quenched state of BPD described above (>90%) is a result of the tightly packed BPD molecules within, and subsequently improves the efficiency of photobleaching by self-oxidation.

Detection of Singlet Oxygen using SOSG and DADB

As photosensitization is a complex process that is influenced by multiple microenvironmental factors, the RMS produced by the irradiation of BPD includes both type I and type II reaction products, namely singlet oxygen, hydroxyl radical, superoxide radical and radical species of BPD itself (44, 45). As singlet oxygen is the predominant cytotoxic RMS produced by the photoirradiation of BPD, we used two separate chemo-selective probes for singlet oxygen, SOSG and DADB. The endoperoxide photooxidation product of SOSG is highly florescent, emitting light around 520 nm, while the DADB endoperoxide photooxidation product is non-fluorescent and exhibits a decay in the emission peak around 500 nm (30). The emission spectra of DADB or SOSG in the absence and presence of BPD and lipo BPD are shown in Figure S3, confirming that BPD fluorescence is negligible at the wavelengths used to monitor DADB and SOSG signals. SOSG is a widely used cell-impermeable probe which is available commercially and provides a sensitive measure of singlet oxygen generation in aqueous environments. However, although SOSG is used widely for evaluating nanoconstructs for PDT (46–48, 9), SOSG suffers from numerous limitations. The most significant limitations include reports that the fluorescent endoperoxide product of SOSG can itself generate singlet oxygen upon excitation (49, 50), its susceptibility to photodecomposition (51) and its inability to diffuse into hydrophobic regions of nanoconstructs that are most commonly used as carriers for PS molecules. Conversely, DADB is a cell-permeable singlet oxygen probe which has been reported for the evaluation of singlet oxygen formation during PDT in cells and was synthesized for this study as previously reported (30). Being a hydrophobic cell permeable molecule, DADB was used in this study as a sensitive probe for singlet oxygen production in hydrophobic

environments, such as the phospholipid bilayer of the nanolipid formulations used here. DADB partitions in the bilayer and thus informs of the immediate singlet oxygen generation in the membrane, without the need for diffusion to the extraliposomal space, as is the case for SOSG.

Interestingly, upon irradiation, no significant differences in the rate of increase of SOSG emission were observed for BPD and its lipidated variants (Figure 6a), or for their nanolipid formulations, except for Visudyne (Figure 6 c, d). Visudyne had the lowest rate of increase in SOSG emission at 0.006 arbitrary units (A.U.)/J.cm^{-2} . This was also hypothesized to be a result of the >90% quenched state of BPD in Visudyne. These observations could be misinformed by the aforementioned concerns with SOSG, and thus must be evaluated in light of those limitation. Intriguingly, the use of DADB as the probe for singlet oxygen yielded a greater variation between the free BPD variants and the nanolipid formulations, in addition to a greater variation between the different types of nanolipid formulations. It is apparent that the hydrophobic partitioning of DADB into the hydrophobic regions of the nanolipid formulations increased the efficiency of endoperoxide formation, as the rate of DADB fluorescence decay in each nanolipid formulation was faster than all of the respective free BPD variant molecules in DMSO, other than for Visudyne and mic BPD-cholesterol. The fastest rate of DADB fluorescence decay was observed with the lipo BPD at 0.105 %/J.cm^{-2} and the slowest was observed with the mic BPD-cholesterol (0.0048 %/J.cm^{-2}), which is hypothesized to be due to the close proximity of the cholesterol moieties within the formulation that quench singlet oxygen. In addition to being a potent lipid anchor, cholesterol is also a critical component of almost all approved nanoliposomes (19). Furthermore, several lipid constituents of the approved Visudyne formulation, including egg phosphatidylglycerol, ascorbyl palmitate and butylated hydroxytoluene are also unsaturated (1). Given the systemic use of such lipids in preclinical and clinical studies using nanolipid formulations for PDT, it is important to include them in these studies in order to evaluate the photochemistry and photophysics of the formulations as a whole, along with the potential chemical quenching interactions. The fact that the conjugation of cholesterol to BPD in the mic BPD-cholesterol formulation did not quench the singlet oxygen that was detected by SOSG implies that the diffusion of singlet oxygen out of the nanolipid formulation to SOSG in solution is a major rate limiting step. The inability of SOSG to diffuse into the hydrophobic regions of the nanolipid formulations of BPD makes it a poor candidate for the sensitive detection of changes in photochemistry, such as the quenching of singlet oxygen by the cholesterol conjugated to BPD.

In all cases for the BPD variants and the respective nanolipid formulations, sodium azide, a physical quencher for singlet oxygen, inhibited the singlet oxygen-mediated increase in SOSG emission and decay in DADB emission (Figure S4). However, sodium azide did not prevent the 16:0 BPD-PC, 20:0 BPD-PC and BPD entrapped in the nanolipid formulations from decreasing the emission of DADB, most likely due to the inability of sodium azide to diffuse through the lipid bilayer (Figure S4c).

Phototoxicity in OVCAR-5 Cells

To assess the importance of the aforementioned photochemical and photophysical parameters investigated in this study in the panel of nanolipid formulations of BPD, phototoxicity was investigated in OVCAR-5 ovarian adenocarcinoma cells. As a result of the potent phototoxicity of Visudyne, lipo BPD and mic BPD-cholesterol, a concentration of 100 nM was sufficient to induce phototoxicity. Lipo 16:0 BPD-PC, Lipo 16:0 BPD-PC and Lipo 16:0 BPD-PC were incubated with the OVCAR-5 cells at 250 nM to deliver effective phototoxicity upon illumination. Following 24 h of incubation, OVCAR-5 cells incubated with the various nanolipid formulations of BPD were irradiated with 690 nm light at 150 mW/cm^2 with varying fluences to deliver PDT dose products (nM BPD equivalent × J/cm^2) from 10 to 15,000, as summarized in Table 1 outlining the BPD concentration equivalents and fluences needed to achieve the aforementioned PDT dose products. 72 h following PDT, viability of the OVCAR-5 cells was assessed by the MTT assay and LD_{50} doses for all nanolipid formulations were determined (Figure 7a; Table 5). Visudyne was found to be the most potent nanolipid PDT agent with an LD_{50} of 755.1 nM × J/cm^2. Lipo BPD proceeded after with an LD_{50} of 1,137.9 nM × J/cm^2. Of the two lysophosphocholine BPD conjugates, the nanolipid formulation of 16:0 BPD-PC was greater than two-fold more potent than that of 20:0 BPD-PC with an LD_{50} of 4,415.8 nM × J/cm^2. This difference was remarkable, as the 20:0 BPD-PC conjugate varies only in 4 additional methylene groups on the lysophospholipid acyl chain, which has no impact on the photophysics or the photochemistry of the nanolipid formulation as compared to the 16:0 BPD-PC counterpart. The least phototoxic nanolipid formulation was the lipo DSPE-PEG-BPD, which surprisingly exhibited the same rates of DADB decay following photoexcitation as lipo 16:0 BPD-PC and lipo 20:0 BPD-PC and retained 57.97% of its photoactivity.

Although the LD_{50} of mic BPD-cholesterol was almost three-fold lower than that of Visudyne at 275.1 nM × J/cm^2, the sustained *ca.* 40% dark toxicity observed skewed the LD_{50} dose of the construct. The dark toxicity of mic BPD-cholesterol was unexpected and appears to be a result of an increased toxicity profile of the BPD-cholesterol conjugate, as compared to the parent molecules BPD and cholesterol. This is further supported by the observation that 100 nM BPD equivalent and 9.58 μM cholesterol equivalent present in the lipo BPD was not toxic to OVCAR-5 cells in the absence of light. The dark toxicity of mic BPD-cholesterol reported here raises concerns regarding the utility of this nanolipid formulation as a PDT agent but can still provide some fundamental insights into the relationship between photochemical and photophysical properties.

By assessing the correlations between the LD_{50} of the various nanolipid formulations tested and the photophysical and photochemical properties (Figure 7b), we found no statistically significant relationship between phototoxicity and the rate of DADB decay (Figure 7c), the rate of increase in SOSG emission (Figure 7d), the rate of photosensitizer photobleaching (Figure 7e), the degree of retention of photoactivity (Figure 7f) or the fluorescence quantum yield (Figure 7g). A positive, statistically significant correlation ($r^2 = 0.9179$, $p < 0.05$) was observed only between the degree of retention of photoactivity within the nanolipid formulation and the rate of increase in SOSG emission.

Interestingly, when monitoring the fluorescence of the panel of nanolipid formulations of BPD in serum containing media, Visudyne was the only formulation to exhibit over 15-fold dequenching over a 24 h incubation period at 37 °C (Figure S5). The fluorescence emission of the remaining nanolipid formulations all remained unchanged over the 24 h incubation period, suggesting that the lipidation promoted stable nanoconstruct insertion. The stark contrast between the marked instability of BPD in the Visudyne formulation and the stability of BPD in the liposomal formulation over 24 hours is not consistent with the fact that both nanolipid formulations were the most potent PDT agents in OVCAR-5 cells. Early work by Aveline *et al.* and Allison *et al.* has determined that BPD readily partitions with human serum albumin and with low density lipoprotein, and in fact, circulates the blood and readily enters cells through receptor-mediated endocytosis as a result of its affinity to these serum proteins (52, 53). Therefore the instability of BPD from the Visudyne formulation alludes to the fact that the BPD entering the cell may not be entirely associated with the nanolipid construct. In light of the complexity of photosensitizer transport and cellular delivery, either free or in nanolipid formulations, a more mechanistic understanding regarding the intracellular fate of BPD and its lipidated variants is critical in guiding the design of novel nanoconstruct for PDT that target specific subcellular compartments.

Conclusions

In this study, a panel of nanolipid formulations has been developed, stably entrapping BPD and a number of variants that have been lipidated, which exhibit differential molecular weights, photophysical and photochemical properties, whilst maintaining the inherent optical properties of the PS. The nanolipid formulations prepared were all stable and monodisperse, with polydispersity indices below 0.2, other than the clinical formulation Visudyne and micellular BPD-cholesterol. Other than Visudyne and micellular BPD-cholesterol, the remaining nanolipid formulations all exhibited moderately negative ζ-potentials (−17 mV to −20 mV), that are known to have favorable pharmacokinetic properties (33, 34). The fluorescence polarization of all the BPD variants is higher in the nanolipid formulations in PBS than as free molecules in DMSO, confirming that they are associated with the lipid constituents of the construct. These nanolipid formulations were then used as model platforms to evaluate their degree of photoactivity, singlet oxygen generation using SOSG and DADB, and rates of photobleaching as a measure of photochemical activity. Of all the photochemical and photophysical properties evaluated, no statistically significant correlation was found with the therapeutic index in OCVAR-5 ovarian cancer cells. The absence of an observed relationship between the photophysics and photochemistry of the nanolipid formulations developed in this study with their potency as photodynamic agents strongly suggests that the design and tuning of such light activatable nanoconstructs for PDT requires more complex and rigorous testing in order to predict their effectiveness.

The findings we present here suggest that it is insufficient to evaluate a nanolipid formulation of a photosensitizer solely by conventional investigations of photoactivity, singlet oxygen generation and photobleaching. This study therefore questions the importance of such methods of photochemical and photophysical evaluation that are routinely performed in the field of photonanomedicine and thus questions the significance of

any observed differences between nanoconstructs being developed. Whilst it is not surprising that the uptake kinetics, subcellular sequestration and molecular targets of PDT mediated by nanotechnology are critical, the apparent lack of relevance of evaluating photophysics and photochemistry in a cell-free system is intriguing. Although not a single factor can be predictive of efficacy, our recent study demonstrates that the subcellular localization of photosensitizers has a marked impact on the efficacy of PDT, with lysosomal targets for photodamage being less phototoxic than photodamage to the mitochondria and endoplasmic reticulum (5). In this recent study, the localization of BPD in the mitochondria and endoplasmic reticulum is contingent on the weak affinity of BPD to its nanolipid formulation, and thus a nanoconstruct containing a stably inserted PS would require more elaborate efforts to target alternative organelles, such as the mitochondria and endoplasmic reticulum. Redirecting nanoconstructs to specific organelles is not trivial, although modulating the endocytic process by which nanoparticles enter cells has been shown to actively target certain organelles (54, 55). Examples include clathrin-mediated endocytosis of ligand targeted nanoconstructs leading to lysosomal sequestration, caveolae-mediated endocytosis leading to redirection to the smooth endoplasmic reticulum or Golgi body, clathrin- and caveolin-independent endocytosis leading to cytosolic delivery and targeting of the endoplasmic reticulum. Functionalization of nanoparticles with organelle targeting moieties has also been reported, with examples including functionalization with nuclear targeting sequences that lead to nuclear sequestration and triphenylphosphonium modification of nanoconstructs for mitochondrial targeting (54–56). These strategies to direct nanoconstruct to various organelles, such as the ER and mitochondria, to improve their efficacy cannot be extended to PDT systems that undergo more complex internalization processes, such as photoactivated uptake, which lead to a tunable localization in cytoplasmic organelle membrane structures and the nucleus (57).

It is essential to note that insights into the molecular mechanisms for PDT may not hold for different cell types, culture methods (*e.g.* 3D models) and *in vivo*. Furthermore, any observed correlations between molecular mechanisms of phototoxicity and therapeutic indices may not be consistent for nanoconstructs containing different photosensitizers and different light irradiances and fluences. Thus, no single parameter alone is expected to be predictive; however, combining mechanistic insights with the photochemical and photophysical parameters, such as those explored in this study, can provide more predictive evaluation workflows to test newly designed nanoconstructs for PDT, especially when tested in *in vitro* models across different cancer indications.

In conclusion, our work reported here underscores the fact that the design of novel nanolipid formulations for PDT must incorporate a mechanistic insight into the photochemical activity within a controlled cellular system, evaluation of subcellular localizations, establishment of sites of photodamage and the mechanisms of cell death in order better predict their potency. This study therefore warrants a future investigation into the relationship between subcellular sites targeted by nanolipid functionalization and subsequent mechanisms of photodamage as additional parameters that serve as more prognostic surrogates for the design and synthesis of more efficacious nanoconstruct for PDT. These studies would ideally be performed in multiple 2D and 3D culture models across multiple disease indications in order to establish

the extent of the consistency between the parameters explored, and between the therapeutic induces observed.

Supplementary Material

Refer to Web version on PubMed Central for supplementary material.

ACKNOWLEDGEMENTS:

This work has been supported in part by the Bullock-Wellman Fellowship and K99CA215301 to G.O.; funding from the China Scholarship Council to W.J.; and NIH support from P01CA084203, R01CA156177, R01CA160998, R21CA220143 to T.H. Excellent technical assistance was provided by Dr. Brijesh Bhayana and Ann Marie Santiago and insightful discussions with Dr. Jerrin Kuriakose and Dr. S. Sibel Erdem are greatly appreciated.

REFERENCES

1. Label VV f. I. F. (NDA 21-119/S-022) Reference ID: 3151429.
2. Huggett MT, Jermyn M, Gillams A, Illing R, Mosse S, Novelli M, Kent E, Bown SG, Hasan T, Pogue BW and Pereira SP (2014) Phase I/II study of verteporfin photodynamic therapy in locally advanced pancreatic cancer. Br. J. Cancer 110, 1698–1704. [PubMed: 24569464]
3. Schmidt-Erfurth U, Hasan T, Gragoudas E, Michaud N, Flotte TJ and Birngruber R (1994) Vascular targeting in photodynamic occlusion of subretinal vessels. Ophthalmology 101, 1953–1961. [PubMed: 7997334]
4. Richter AM, Waterfield E, Jain AK, Canaan AJ, Allison BA and Levy JG (1993) Liposomal delivery of a photosensitizer, benzoporphyrin derivative monoacid ring A (BPD), to tumor tissue in a mouse tumor model. Photochem. Photobiol 57, 1000–1006. [PubMed: 8367528]
5. Rizvi I, Obaid G, Bano S, Hasan T and Kessel D (2018) Photodynamic therapy: Promoting in vitro efficacy of photodynamic therapy by liposomal formulations of a photosensitizing agent. Lasers Surg. Med
6. Huang HC, Rizvi I, Liu J, Anbil S, Kalra A, Lee H, Baglo Y, Paz N, Hayden D, Pereira S, Pogue BW, Fitzgerald J and Hasan T (2018) Photodynamic Priming Mitigates Chemotherapeutic Selection Pressures and Improves Drug Delivery. Cancer Res 78, 558–571. [PubMed: 29187403]
7. Spring BQ, Sears RB, Zheng LZ, Mai Z, Watanabe R, Sherwood ME, Schoenfeld DA, Pogue BW, Pereira SP and Villa E (2016) A photoactivable multi-inhibitor nanoliposome for tumour control and simultaneous inhibition of treatment escape pathways. Nat. Nanotechnol 11, 378. [PubMed: 26780659]
8. Obaid G, Broekgaarden M, Bulin AL, Huang HC, Kuriakose J, Liu J and Hasan T (2016) Photonanomedicine: a convergence of photodynamic therapy and nanotechnology. Nanoscale 8, 12471–12503. [PubMed: 27328309]
9. He C, Duan X, Guo N, Chan C, Poon C, Weichselbaum RR and Lin W (2016) Core-shell nanoscale coordination polymers combine chemotherapy and photodynamic therapy to potentiate checkpoint blockade cancer immunotherapy. Nat. Commun 7, 12499. [PubMed: 27530650]
10. Lovell JF, Jin CS, Huynh E, Jin H, Kim C, Rubinstein JL, Chan WC, Cao W, Wang LV and Zheng G (2011) Porphysome nanovesicles generated by porphyrin bilayers for use as multimodal biophotonic contrast agents. Nat. Mater 10, 324–332. [PubMed: 21423187]
11. Jermyn M, Davis SC, Dehghani H, Huggett MT, Hasan T, Pereira SP, Bown SG and Pogue BW (2014) CT contrast predicts pancreatic cancer treatment response to verteporfin-based photodynamic therapy. Phys. Med. Biol 59, 1911–1921. [PubMed: 24651456]
12. Ginevra F, Biffanti S, Pagnan A, Biolo R, Reddi E and Jori G (1990) Delivery of the tumour photosensitizer zinc(II)-phthalocyanine to serum proteins by different liposomes: studies in vitro and in vivo. Cancer Lett 49, 59–65. [PubMed: 2302697]
13. Kiesslich T, Berlanda J, Plaetzer K, Krammer B and Berr F (2007) Comparative characterization of the efficiency and cellular pharmacokinetics of Foscan- and Foslip-based photodynamic treatment

in human biliary tract cancer cell lines. Photochem. Photobiol. Sci 6, 619–627. [PubMed: 17549263]

14. Lassalle H-P, Dumas D, Gräfe S, D'Hallewin M-A, Guillemin F and Bezdetnaya L (2009) Correlation between in vivo pharmacokinetics, intratumoral distribution and photodynamic efficiency of liposomal mTHPC. J. Controlled Release 134, 118–124.
15. Nunes SM, Sguilla FS and Tedesco AC (2004) Photophysical studies of zinc phthalocyanine and chloroaluminum phthalocyanine incorporated into liposomes in the presence of additives. Braz. J. Med. Biol. Res 37, 273–284. [PubMed: 14762584]
16. Reddi E, Zhou C, Biolo R, Menegaldo E and Jori G (1990) Liposome-or LDL-administered Zn (II)-phthalocyanine as a photodynamic agent for tumours. I. Pharmacokinetic properties and phototherapeutic efficiency. Br. J. Cancer 61, 407. [PubMed: 2328207]
17. Komatsu T, Moritake M, Nakagawa A and Tsuchida E (2002) Self-organized lipid-porphyrin bilayer membranes in vesicular form: nanostructure, photophysical properties, and dioxygen coordination. Chemistry 8, 5469–5480. [PubMed: 12561319]
18. Luo D, Carter KA, Razi A, Geng J, Shao S, Giraldo D, Sunar U, Ortega J and Lovell JF (2016) Doxorubicin encapsulated in stealth liposomes conferred with light-triggered drug release. Biomaterials 75, 193–202. [PubMed: 26513413]
19. Achalkumar AS, Bushby RJ and Evans SD (2010) Cholesterol-based anchors and tethers for phospholipid bilayers and for model biological membranes. Soft Matter 6, 6036–6051.
20. Vankayala R, Sagadevan A, Vijayaraghavan P, Kuo CL and Hwang KC (2011) Metal nanoparticles sensitize the formation of singlet oxygen. Angew. Chem. Int. Ed. Engl 50, 10640–10644. [PubMed: 21932210]
21. Cheng Y, Cheng H, Jiang C, Qiu X, Wang K, Huan W, Yuan A, Wu J and Hu Y (2015) Perfluorocarbon nanoparticles enhance reactive oxygen levels and tumour growth inhibition in photodynamic therapy. Nat. Commun 6, 8785. [PubMed: 26525216]
22. Obaid G, Chambrier I, Cook MJ and Russell DA (2012) Targeting the oncofetal Thomsen-Friedenreich disaccharide using jacalin-PEG phthalocyanine gold nanoparticles for photodynamic cancer therapy. Angew. Chem. Int. Ed. Engl 51, 6158–6162. [PubMed: 22573473]
23. Obaid G, Chambrier I, Cook MJ and Russell DA (2015) Cancer targeting with biomolecules: a comparative study of photodynamic therapy efficacy using antibody or lectin conjugated phthalocyanine-PEG gold nanoparticles. Photochem. Photobiol. Sci 14, 737–747. [PubMed: 25604735]
24. Zhao B, Yin JJ, Bilski PJ, Chignell CF, Roberts JE and He YY (2009) Enhanced photodynamic efficacy towards melanoma cells by encapsulation of Pc4 in silica nanoparticles. Toxicol. Appl. Pharmacol 241, 163–172. [PubMed: 19695274]
25. Sebak AA, Gomaa II, ElMeshad AN and AbdelKader MH (2018) Targeted Photodynamic-Induced Singlet Oxygen Production by Peptide-Conjugated Biodegradable Nanoparticles for Treatment of Skin Melanoma. Photodiagnosis Photodyn. Ther
26. Khan S, Alam F, Azam A and Khan AU (2012) Gold nanoparticles enhance methylene blue-induced photodynamic therapy: a novel therapeutic approach to inhibit Candida albicans biofilm. Int. J. Nanomedicine 7, 3245–3257. [PubMed: 22802686]
27. Anbil S, Rizvi I, Celli J, Alagic N and Hasan T A photobleaching-based PDT dose metric predicts PDT efficacy over certain BPD concentration ranges in a three-dimensional model of ovarian cancer. Vol. 8568, pp. 85680S International Society for Optics and Photonics, Proceedings of the Optical Methods for Tumor Treatment and Detection: Mechanisms and Techniques in Photodynamic Therapy XXII2013.
28. Jarvi MT, Patterson MS and Wilson BC (2012) Insights into photodynamic therapy dosimetry: simultaneous singlet oxygen luminescence and photosensitizer photobleaching measurements. Biophysical J 102, 661–671.
29. Zhang P, Steelant W, Kumar M and Scholfield M (2007) Versatile photosensitizers for photodynamic therapy at infrared excitation. J. Am. Chem. Soc 129, 4526–4527. [PubMed: 17385866]

30. Kessel D and Price M (2012) Evaluation of Diethyl-3-3′-(9, 10-anthracenediyl) bis Acrylate as a Probe for Singlet Oxygen Formation during Photodynamic Therapy. Photochem. Photobiol 88, 717–720. [PubMed: 22296586]

31. Huang HC, Mallidi S, Liu J, Chiang CT, Mai Z, Goldschmidt R, Ebrahim-Zadeh N, Rizvi I and Hasan T (2016) Photodynamic Therapy Synergizes with Irinotecan to Overcome Compensatory Mechanisms and Improve Treatment Outcomes in Pancreatic Cancer. Cancer Res 76, 1066–1077. [PubMed: 26719532]

32. Bhattacharjee S (2016) DLS and zeta potential–What they are and what they are not? J. Controlled Release 235, 337–351.

33. Awasthi VD, Garcia D, Klipper R, Goins BA and Phillips WT (2004) Neutral and anionic liposome-encapsulated hemoglobin: effect of postinserted poly(ethylene glycol)-distearoylphosphatidylethanolamine on distribution and circulation kinetics. J. Pharmacol. Exp. Ther 309, 241–248. [PubMed: 14718581]

34. Krasnici S, Werner A, Eichhorn ME, Schmitt-Sody M, Pahernik SA, Sauer B, Schulze B, Teifel M, Michaelis U, Naujoks K and Dellian M (2003) Effect of the surface charge of liposomes on their uptake by angiogenic tumor vessels. Int. J. Cancer 105, 561–567. [PubMed: 12712451]

35. Aveline BM, Hasan T and Redmond RW (1995) The effects of aggregation, protein binding and cellular incorporation on the photophysical properties of benzoporphyrin derivative monoacid ring A (BPDMA). J. Photochem. Photobiol. B 30, 161–169. [PubMed: 8558368]

36. Papahadjopoulos D, Jacobson K, Nir S and Isac T (1973) Phase transitions in phospholipid vesicles. Fluorescence polarization and permeability measurements concerning the effect of temperature and cholesterol. Biochim. Biophys. Acta. 311, 330–348. [PubMed: 4729825]

37. Redmond RW, Kochevar IE, Krieg M, Smith G and McGimpsey WG (1997) Excited state relaxation in cyanine dyes: a remarkably efficient reverse intersystem crossing from upper triplet levels. J. Phys. Chem. A 101, 2773–2777.

38. Bonnett R and Martınez G (2001) Photobleaching of sensitisers used in photodynamic therapy. Tetrahedron. 57, 9513–9547.

39. Potter WR, Mang T and Dougherty T (1987) The theory of photodynamic therapy dosimetry: consequences of photo-destruction of sensitizer. Photochem. Photobiol 46, 97–101. [PubMed: 2956621]

40. Mang TS, Dougherty TJ, Potter WR, Boyle DG, Somer S and Moan J (1987) Photobleaching of porphyrins used in photodynamic therapy and implications for therapy. Photochem. Photobiol 45, 501–506. [PubMed: 3575444]

41. Celli JP, Spring BQ, Rizvi I, Evans CL, Samkoe KS, Verma S, Pogue BW and Hasan T (2010) Imaging and photodynamic therapy: mechanisms, monitoring, and optimization. Chem. Rev 110, 2795–2838. [PubMed: 20353192]

42. Wilson BC, Patterson MS and Lilge L (1997) Implicit and explicit dosimetry in photodynamic therapy: a New paradigm. Lasers Med. Sci 12, 182–199. [PubMed: 20803326]

43. Rizvi I, Anbil S, Alagic N, Celli J, Zheng LZ, Palanisami A, Glidden MD, Pogue BW and Hasan T (2013) PDT dose parameters impact tumoricidal durability and cell death pathways in a 3D ovarian cancer model. Photochem. Photobiol 89, 942–952. [PubMed: 23442192]

44. Hadjur C, Wagnieres G, Monnier P and Bergh H (1997) EPR and Spectrophotometric Studies of Free Radicals (O2°−,° OH, BPD-MA°−) and Singlet Oxygen (1O2) Generated by Irradiation of Benzoporphyrin Derivative Monoacid Ring A. Photochem. Photobiol 65, 818–827.

45. Price M, Reiners JJ, Santiago AM and Kessel D (2009) Monitoring singlet oxygen and hydroxyl radical formation with fluorescent probes during photodynamic therapy. Photochem. Photobiol 85, 1177–1181. [PubMed: 19508643]

46. Dou QQ, Teng CP, Ye E and Loh XJ (2015) Effective near-infrared photodynamic therapy assisted by upconversion nanoparticles conjugated with photosensitizers. Int. J. Nanomedicine 10, 419–432. [PubMed: 25609954]

47. Huang P, Li Z, Lin J, Yang D, Gao G, Xu C, Bao L, Zhang C, Wang K and Song H (2011) Photosensitizer-conjugated magnetic nanoparticles for in vivo simultaneous magnetofluorescent imaging and targeting therapy. Biomaterials 32, 3447–3458. [PubMed: 21303717]

48. Xiao L, Gu L, Howell SB and Sailor MJ (2011) Porous silicon nanoparticle photosensitizers for singlet oxygen and their phototoxicity against cancer cells. ACS Nano 5, 3651–3659. [PubMed: 21452822]

49. Gollmer A, Arnbjerg J, Blaikie FH, Pedersen BW, Breitenbach T, Daasbjerg K, Glasius M and Ogilby PR (2011) Singlet Oxygen Sensor Green(R): photochemical behavior in solution and in a mammalian cell. Photochem. Photobiol 87, 671–679. [PubMed: 21272007]

50. Koh E and Fluhr R (2016) Singlet oxygen detection in biological systems: Uses and limitations. Plant Signal. Behav 11, e1192742. [PubMed: 27231787]

51. Kim S, Fujitsuka M and Majima T (2013) Photochemistry of singlet oxygen sensor green. J. Phys. Chem. B 117, 13985–13992. [PubMed: 24111566]

52. Aveline BM, Hasan T and Redmond RW (1995) The effects of aggregation, protein binding and cellular incorporation on the photophysical properties of benzoporphyrin derivative monoacid ring A (BPDMA). J. Photochem. Photobiol., B 30, 161–169. [PubMed: 8558368]

53. Allison BA, Pritchard PH and Levy JG (1994) Evidence for low-density lipoprotein receptor-mediated uptake of benzoporphyrin derivative. Br. J. Cancer 69, 833–839. [PubMed: 8180011]

54. Sakhrani NM and Padh H (2013) Organelle targeting: third level of drug targeting. Drug Des. Devel. Ther 7, 585–599.

55. Biswas S and Torchilin VP (2014) Nanopreparations for organelle-specific delivery in cancer. Adv. Drug Deliv. Rev 66, 26–41. [PubMed: 24270008]

56. Wang Z, Kuang X, Shi J, Guo W and Liu H (2017) Targeted delivery of geranylgeranylacetone to mitochondria by triphenylphosphonium modified nanoparticles: a promising strategy to prevent aminoglycoside-induced hearing loss. Biomater Sci 5, 1800–1809. [PubMed: 28650045]

57. Svensson FR, Matson M, Li M and Lincoln P (2010) Lipophilic ruthenium complexes with tuned cell membrane affinity and photoactivated uptake. Biophys. Chem 149, 102–106. [PubMed: 20471741]

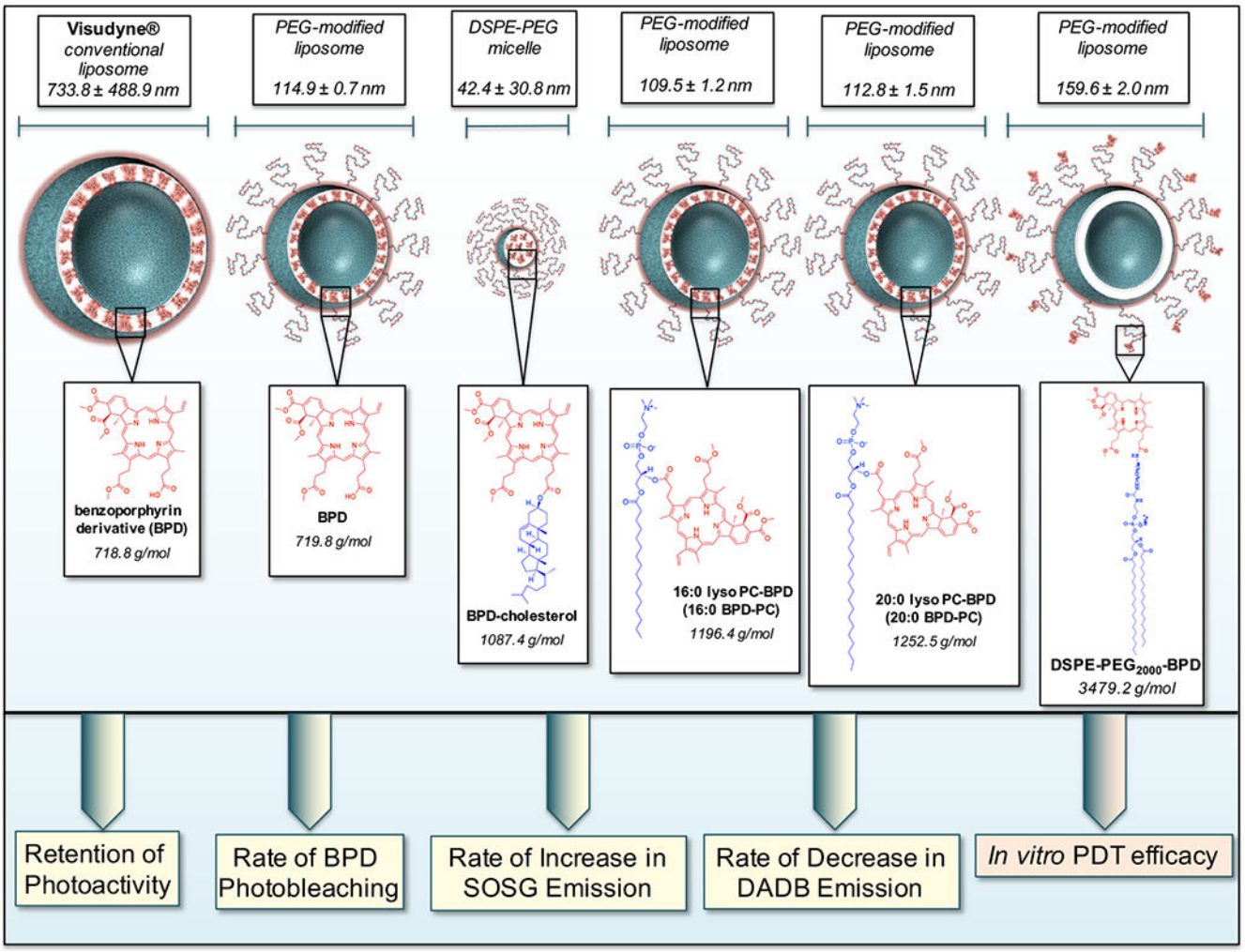

Figure 1.

Graphical representation of the panel of BPD-based nanolipid formulations investigated in this study with the respective hydrodynamic diameters (nm) determined using dynamic light scattering. Chemical structures of BPD, BPD-cholesterol, 16:0 BPD-PC, 20:0 BPD-PC and DSPE-PEG-BPD entrapped in the nanolipid formulations are presented for the respective constructs. The photoactivity, photobleaching, singlet oxygen production (as a function of increased Singlet Oxygen Sensor Green (SOSG) emission and decreased diethyl-3-3′-(9,10-anthracenediyl)bis Acrylate (DADB) emission) of the BPD-based nanolipid formulations will be evaluated with respect to their *in vitro* PDT efficacy in OVCAR-5 cells.

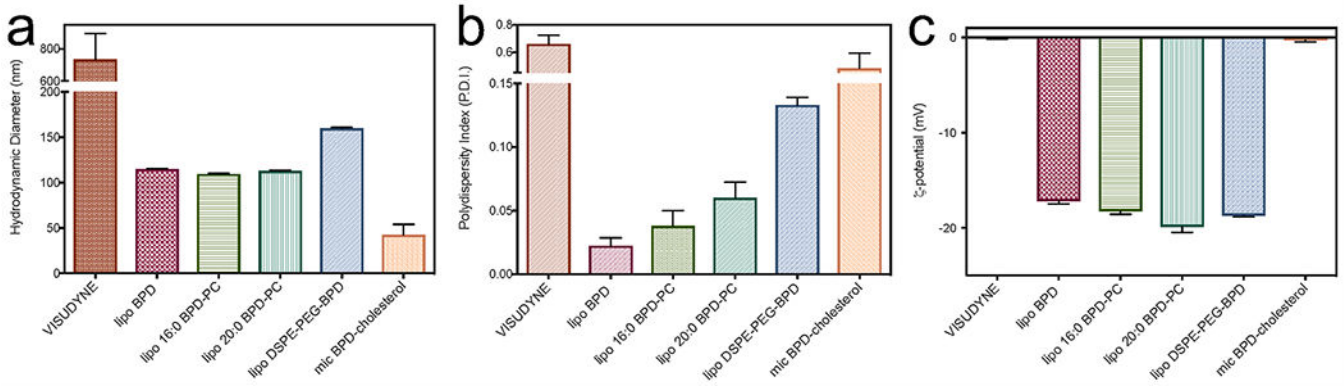

Figure 2.

Dynamic Light Scattering analysis of the nanolipid formulations of BPD and its lipidated variants portraying hydrodynamic diameter (a), polydispersity indices (P.D.I.'s; b) and ζ-potential (c) of all constructs.

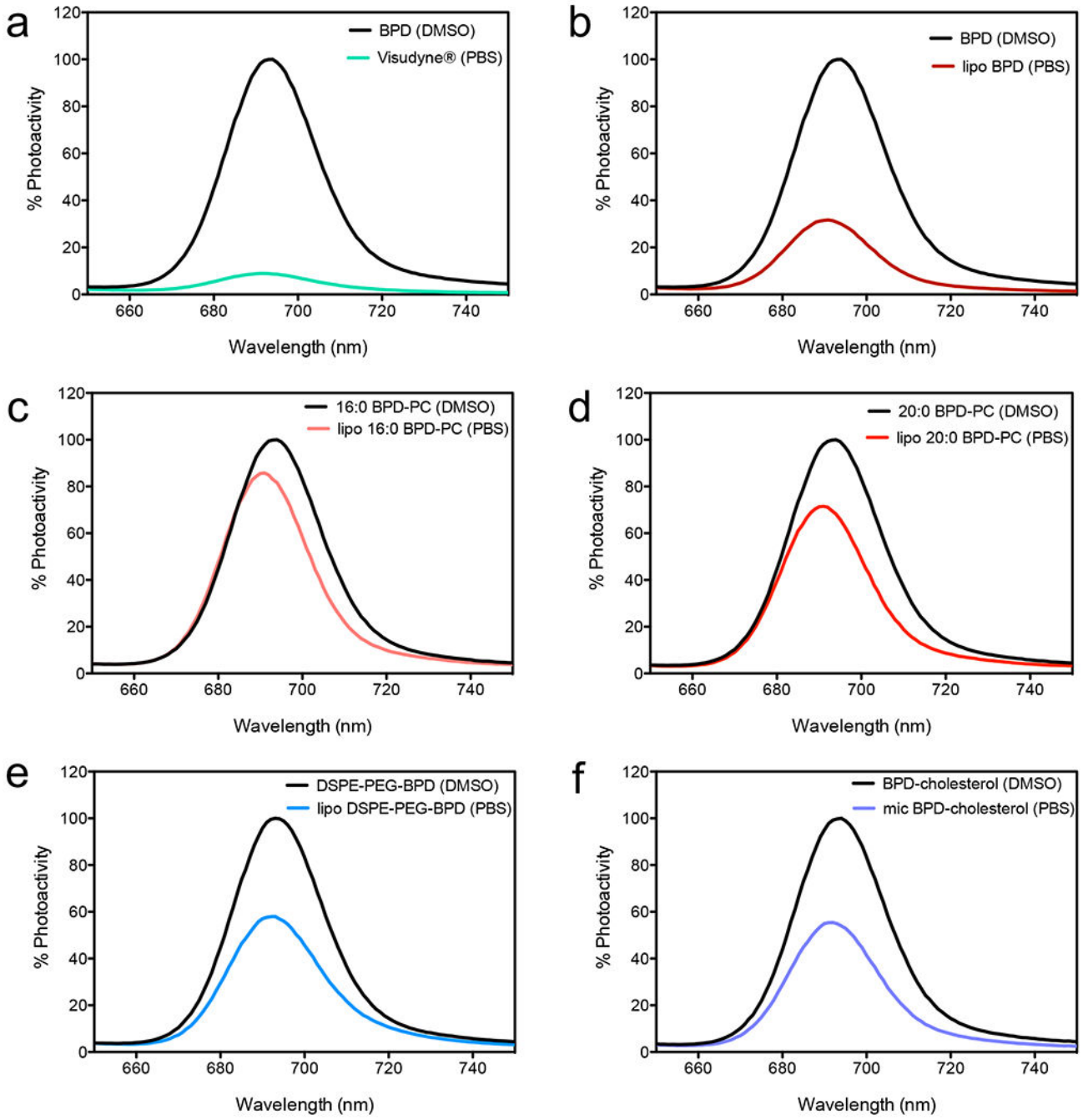

Figure 3.

Fluorescence emission spectra of BPD and its lipid conjugates in DMSO or as nanolipid formulation. An excitation wavelength at 435 nm was used for all preparations and the spectra are mean emission intensities (n=4).

a

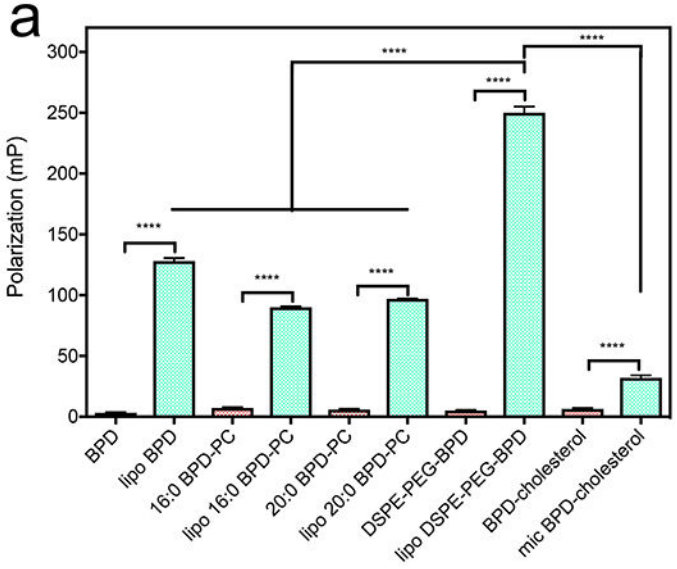

b

BPD Variant	Mean Polarization (mP)	S.D.	Solvent
BPD	3.3	0.8	DMSO
lipo BPD	128	4.5	PBS
16:0 BPD PC	7.3	1.1	DMSO
lipo 16:0 BPD-PC	90	1.5	PBS
20:0 BPD-PC	5.9	1.2	DMSO
lipo 20:0 BPD-PC	97	0.5	PBS
DSPE-PEG-BPD	5.1	0.9	DMSO
lipo DSPE-PEG-BPD	250	9	PBS
BPD-cholesterol	6.5	1.3	DMSO
mic BPD-cholesterol	32	3.5	PBS
BPD (reference)	245	26	glycerol
BPD (reference)	3.5	1.4	methanol

Figure 4.

a) Fluorescence polarization of BPD and its lipidated variants in DMSO and of the respective nanoformulations in PBS. (Values are mean ± S.D., n=3) b) Summary of all fluorescence polarization measurements of BPD and its lipidated variants including reference measurements of BPD in glycerol and methanol.

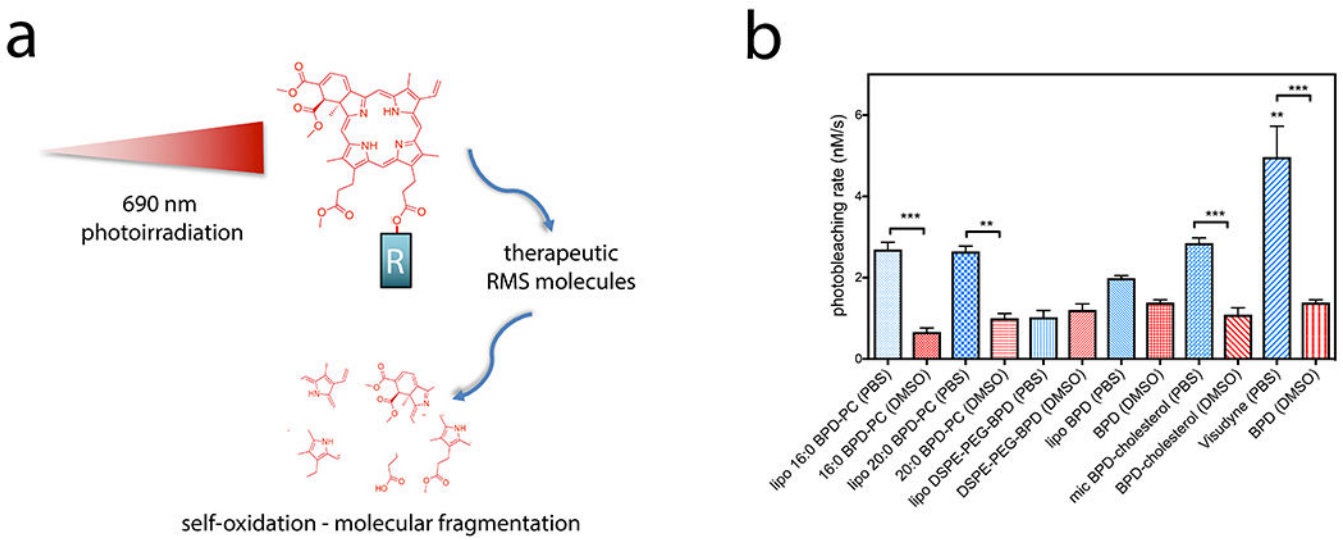

Figure 5.

a) Graphical representation of self-oxidation and photobleaching of BPD and its lipidated derivatives by the production of reactive molecular species (RMS) following photoirradiation using 690 nm laser light. ‘R’ indicates either a hydroxyl group of the carboxylate in native BPD, or the lipids conjugated in the lipidated variants. Self-oxidation leads to molecular fragmentation of the PS molecule, resulting in permanent photobleaching. b) Rates of photobleaching of BPD or its lipidated derivatives free in DMSO or entrapped in nanolipid formulations in PBS. (Statistical analysis performed by One-way ANOVA with a Tukey Post-Test. Values are mean ± S.E.M., n=4)

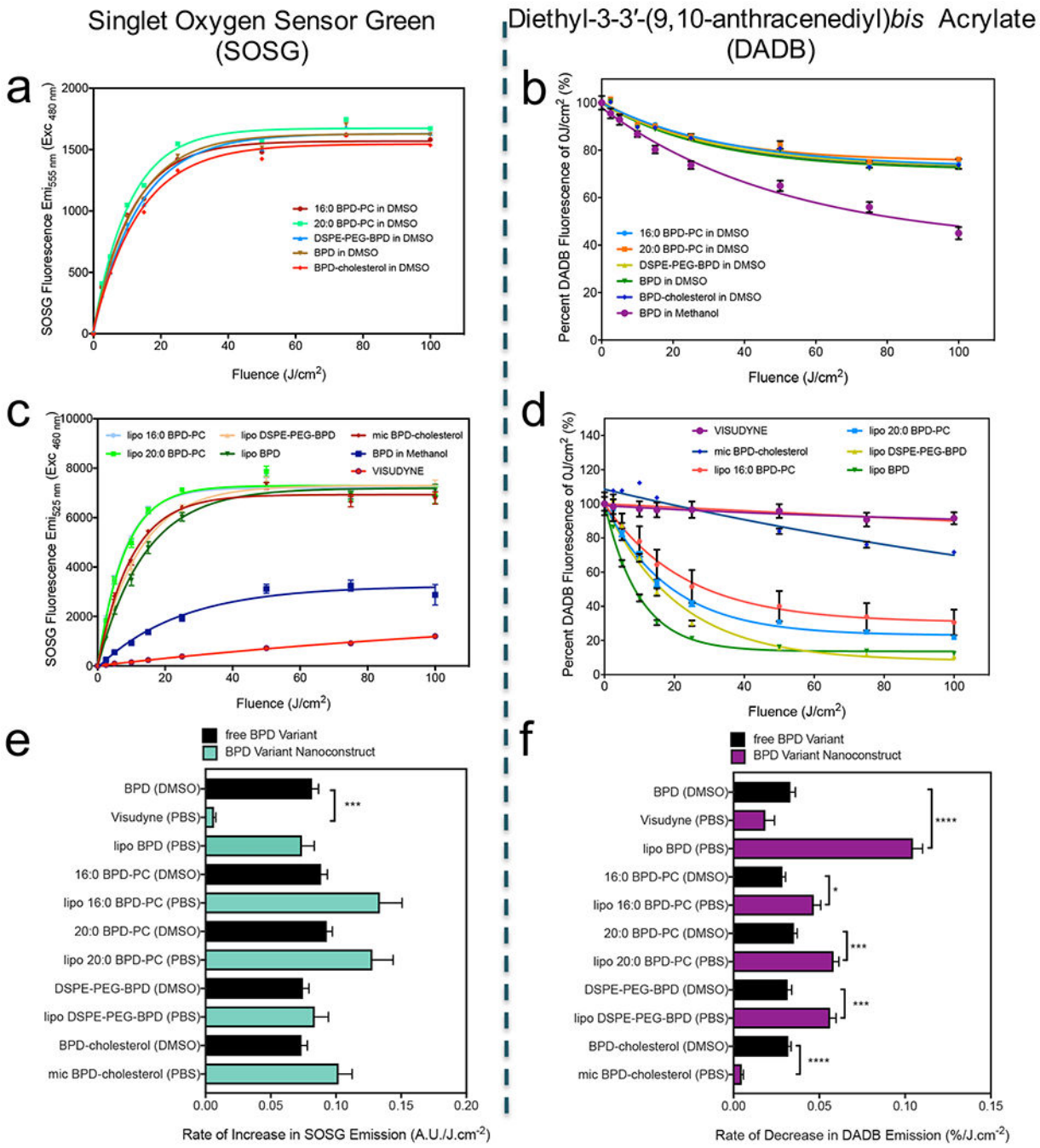

Figure 6.

SOSG Emission with increasing fluences of 690 nm light irradiation of BPD and its lipid variants (a), in addition to their respective nanolipid formulations (b). Diethyl-3-3′-(9,10-anthracenediyl)*bis* Acrylate (DADB) (mean = ± SEM)

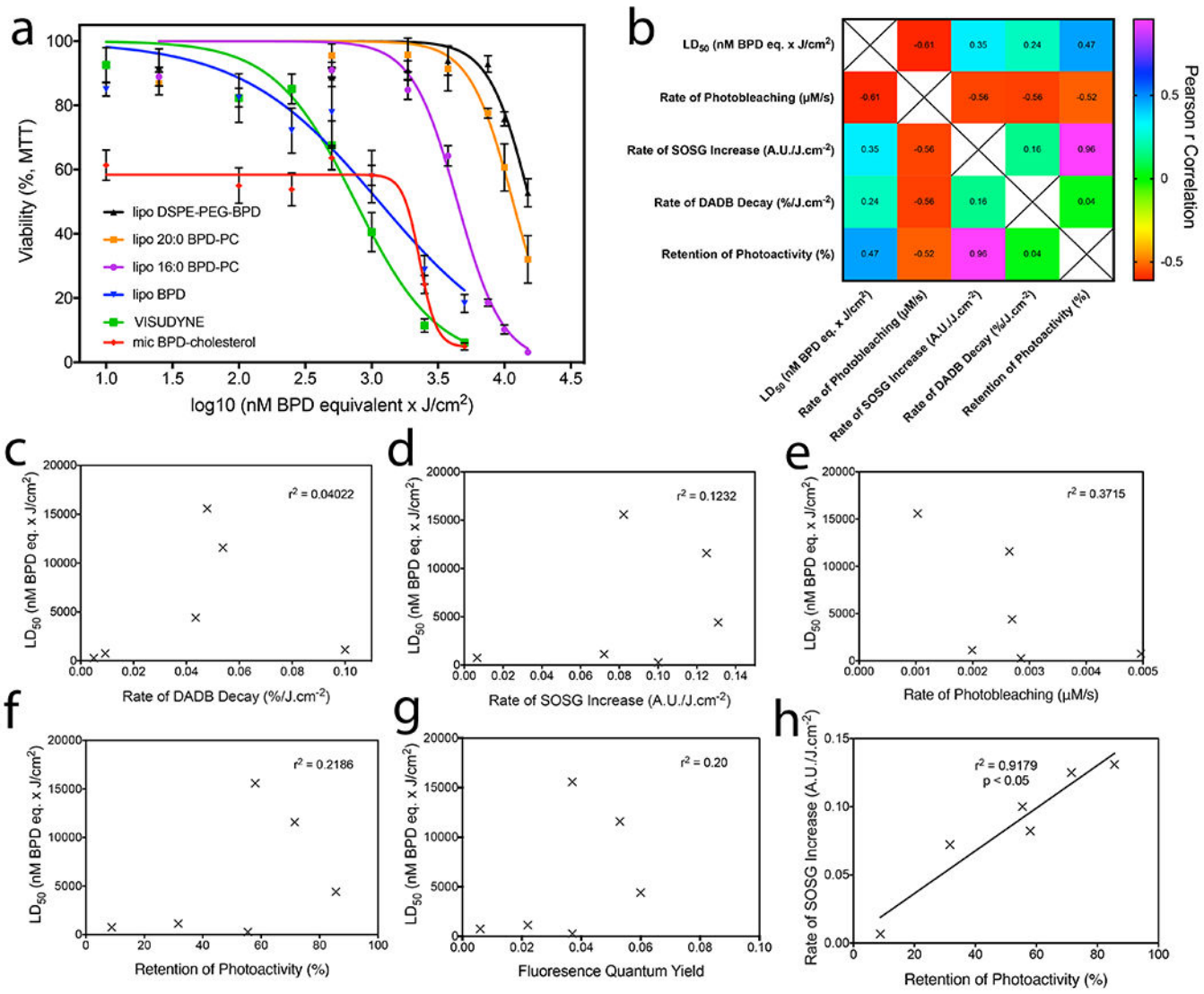

Figure 7.

a) Survival curves of OVCAR-5 cells obtained using the MTT viability assay 72h following PDT with varying fluences of 690 nm light at an irradiance of 150 mW/cm^2 to deliver PDT dose products of 10 – 15,000 nM BPD equivalent × J/cm^2. b) Pearson's r correlation matrix of nanolipid formulation LD_{50} values in OVCAR-5 cells with their respective photochemical and photophysical properties. Individual plots are represented for LD_{50} values with rates of DADB decay (c), rate of SOSG increase (d), rate of photobleaching (e), degree of retention of photoactivity (f), and fluorescence quantum yield (g). The only statistically significant correlation exists between the degree of retention of photoactivity and rate of SOSG increase (h, $r^2 = 0.9179$, $p<0.05$).

Table 1.

Relationship between the concentrations of BPD equivalent, fluence applied at 150 mW/cm^2 and the respective PDT Dose Product used for comparing the efficacies of all nanolipid formulations.

Nanolipid Formulation	Concentration of BPD Equivalent (nM)	Fluence (J/cm^2)	Respective PDT Dose Product (nM BPD eq. × J/cm^2)
mic BPD-cholesterol, Visudyne, lipo BPD	100	0.1	10
	100	1	100
	100	2.5	250
	100	5	500
	100	10	1000
	100	25	2500
	100	50	5000
lipo 16:0 BPD-PC, lipo 20:0 BPD-PC, lipo DSPE-PEG-BPD	250	0.1	25
	250	2	500
	250	7.5	1875
	250	15	3750
	250	30	7500
	250	40	10000
	250	60	15000

Table 2.

Observed (MALDI) and expected masses of BPD and its lipidated variants with their respective purity levels, as assessed by HPLC.

BPD Variant	Observed Mass (m/z)	Expected Mass (g/mol)	Purity by HPLC (%)	Retention Time (min)
BPD	719.738	718.79	99.17	23.5
16:0 BPD-PC	1198.791	1196.41	99.15	34.89
20:0 BPD-PC	1254.965	1252.52	98.30	41.71
BPD-cholesterol	1087.111	1087.43	97.37	44.43
DSPE-PEG-BPD	3630.591	3479.25	97.86	38.83

Table 3.

Summary of the physical characterization of BPD and its lipid variants entrapped within nanolipid formulations. Values are mean (± S.D.)

Nanolipid Formulation	Hydrodynamic Diameter (nm)	Polydispersity Index (P.D.I.)	Potential (mV)
Visudyne	733.78 (488.87)	0.66 (0.20)	0.16 (0.21)
lipo BPD	114.90 (0.72)	0.02 (0.01)	−17.17 (0.49)
lipo 16:0 BPD-PC	109.50 (1.18)	0.038 (0.02)	−18.23 (0.59)
lipo 20:0 BPD-PC	112.83 (1.53)	0.06 (0.02)	−19.87 (1.01)
lipo DSPE-PEG-BPD	159.63 (2.02)	0.13 (0.01)	−18.70 (0.26)
mic BPD-cholesterol	42.42 (30.75)	0.48 (0.30)	−0.28 (0.35)

Table 4.

A summary of the optical properties of BPD and its lipid variants as free molecules dissolved in DSMO, or as nanolipid formulations in PBS.

BPD Variant	Solvent	Emi_{max} (nm)	Photoactivity Retained by Nanoformulation (%)	Fluorescence Quantum Yield (Φ)
BPD	Methanol	689	*n.a.*	0.051 *
BPD	DMSO	694	n.a.	0.069
Visudyne	PBS	691	8.83	0.006
lipo BPD	PBS	691	31.64	0.022
16:0 BPD-PC	DMSO	694	n.a.	0.070
lipo 16:0 BPD-PC	PBS	690	85.6	0.060
20:0 BPD-PC	DMSO	694	n.a.	0.074
lipo 20:0 BPD-PC	PBS	691	71.48	0.053
DSPE-PEG-BPD	DMSO	693	n.a.	0.064
lipo DSPE-PEG-BPD	PBS	693	57.97	0.037
BPD-cholesterol	DMSO	694	n.a.	0.067
mic BPD-cholesterol	PBS	692	55.42	0.037

* (26) The nanolipid formulations of BPD and its lipidated variants are italicized for clarity

Table 5.

Summary of the physical characterization of BPD and its lipid variants entrapped within nanolipid formulations.

Nanolipid Formulation	Mean LD_{50} (nM BPD eq. × J/cm^2)
mic BPD-cholesterol	275.08
Visudyne	755.08
lipo BPD	1,137.93
lipo 16:0 BPD-PC	4,415.82
lipo 20:0 BPD-PC	11,585.34
lipo DSPE-PEG-BPD	15,588.73